

# MAASS FORM $L$ -FUNCTIONS

DAVID W. FARMER AND STEFAN LEMURELL

ABSTRACT. We present examples of Maass forms on Hecke congruence groups, giving low eigenvalues on  $\Gamma_0(p)$  for small prime  $p$ , and the first 1000 eigenvalues for  $\Gamma_0(11)$ . We also present calculations of the  $L$ -functions associated to the Maass forms and make comparisons to the predictions from random matrix theory.

## 1. INTRODUCTION

Much recent progress in understanding  $L$ -functions has come from the idea of a “family” of  $L$ -functions with an associated symmetry type [KSa]. The idea is that to a naturally occurring collection of  $L$ -functions one can associate a classical compact group: unitary, symplectic, or orthogonal. One expects the analytic properties of the  $L$ -functions to be largely governed by the symmetry type. That is, averages over the family of  $L$ -functions should equal averages with respect to Haar measure over the matrix group. This philosophy has produced a wealth of interesting predictions which have been confirmed both theoretically and numerically. See [CFKRS] for an extensive discussion.

The family of  $L$ -functions of interest to us here is the collection of  $L$ -functions associated to Maass forms. Specifically, for a given Hecke congruence group  $\Gamma = \Gamma_0(N)$ , we consider the Maass forms on  $\Gamma$  and the  $L$ -functions associated to those Maass forms. This constitutes an “orthogonal” family of  $L$ -functions, and this leads to some specific predictions about statistical properties of the critical values and the zeros of the  $L$ -functions. While examples of  $L$ -functions associated to Maass forms have been evaluated before [S], in this paper we provide the first numerical tests of the random matrix predictions by finding the first 1000 newform Maass forms on  $\Gamma_0(11)$  and computing the associated  $L$ -functions. We also test standard predictions about the statistics of those eigenvalues, and we find the first few eigenvalues on  $\Gamma_0(p)$  for small  $p$ .

In the next section we recall properties of Maass forms and their associated  $L$ -functions. In section 3 we describe our algorithm for locating and computing Maass forms. We then present the results of our calculations, in section 4 addressing the low eigenvalues on  $\Gamma_0(p)$ , and in section 5 the first 1000 eigenvalues for  $\Gamma_0(11)$ . In section 6 we give example plots of Maass  $L$ -functions and discuss their general features. In section 7 we compare the random matrix predictions to our  $L$ -function data. Finally, in section 8 we describe how the  $L$ -functions were computed.

---

Research of the first author supported by the American Institute of Mathematics and the NSF Focused Research Group grant DMS 0244660. Research of the second author supported in part by “Stiftelsen för internationalisering av högre utbildning och forskning” (STINT) .

2. MAASS FORMS AND THEIR  $L$ -FUNCTIONS

The  $L$ -functions we consider are obtained from Maass forms on the Hecke congruence group  $\Gamma_0(11)$ . We first recall the definition of Maass form, and then describe the connection with  $L$ -functions. A good reference on Maass forms is Iwaniec's book [Iw].

**2.1. Maass forms.** A *Maass form* on a group  $\Gamma \subset PSL(2, \mathbb{R})$  is a function  $f : \mathcal{H} \rightarrow \mathbb{R}$  which satisfies:

- (1.1)  $f(\gamma z) = f(z)$  for all  $\gamma \in \Gamma$ ,
- (1.2)  $f$  vanishes at the cusps of  $\Gamma$ , and
- (1.3)  $\Delta f = \lambda f$  for some  $\lambda > 0$ ,

where

$$\Delta = -y^2 \left( \frac{\partial^2}{\partial x^2} + \frac{\partial^2}{\partial y^2} \right)$$

is the Laplace–Beltrami operator on  $\mathcal{H}$ . We set  $\lambda = \frac{1}{4} + R^2$ .

In number theory, Maass forms most commonly arise on Hecke congruence groups:

$$\Gamma_0(N) = \left\{ \begin{pmatrix} a & b \\ c & d \end{pmatrix} \in PSL(2, \mathbb{Z}) : N|c \right\}.$$

Here we consider newforms on  $\Gamma_0(N)$ . This implies that

$$(2.1) \quad \boxed{\text{eqn:fourier}} \quad f(z) = \sum_{n=1}^{\infty} a_n \sqrt{y} K_{iR}(2\pi ny) SC(2\pi nx),$$

where  $K_\nu(\cdot)$  is the  $K$ -Bessel function and  $SC(x)$  is either  $\sin(x)$  or  $\cos(x)$ . In the first case we say that  $f$  is “odd” and in the second  $f$  is “even.” Furthermore,  $f$  is an eigenfunction of the Fricke involution

$$(2.2) \quad \boxed{\text{eqn:fricke}} \quad f(z) = \pm f \left( -\frac{1}{Nz} \right),$$

and  $f$  is also a simultaneous eigenfunction of the Hecke operators  $T_p$  for  $p \nmid N$ . A good introduction to this material is [Iw]. In this paper we only use the properties which are explicitly described above.

If  $M|N$  then  $\Gamma_0(N) \subset \Gamma_0(M)$ . In particular, if  $f(z)$  is a Maass form on  $\Gamma_0(M)$  then  $f(kz)$  is a Maass form on  $\Gamma_0(N)$  for all  $k|(N/M)$ . Such functions are called “oldforms” on  $\Gamma_0(M)$  and it is natural to avoid such functions in a search for Maass forms, for they naturally belong on the larger group. The Maass forms which naturally live on  $\Gamma_0(M)$ , called “newforms”, have a simple characterization in terms of their Fourier coefficients and we only search for newforms in our calculations.

In this paper we consider Maass forms on  $\Gamma_0(p)$  for  $p$  prime. In this case there are four symmetry types:  $(\text{even}, +)$ ,  $(\text{even}, -)$ ,  $(\text{odd}, +)$ , and  $(\text{odd}, -)$ . For  $p \leq 107$  we exhibit the first eigenvalue in each symmetry type, and we found the first 1000 newform eigenvalues on  $\Gamma_0(11)$ . Note that for these calculations we can treat  $\Gamma_0(p)$  as a group with one cusp. This is because the Fricke involution (2.2) switches the cusps 0 and  $\infty$ , and a Fourier expansion of the form (2.1) vanishes at  $\infty$ . However, this simplification is merely a convenience and our methods of computing Maass forms works for arbitrary cofinite subgroups of  $SL(2, \mathbb{R})$ .

**2.2. Maass form  $L$ -functions.** Maass forms originally arose through their connection to  $L$ -functions. If  $f$  is an even Maass form then

$$(2.3) \quad \int_0^\infty f(iy)y^{s-\frac{3}{2}} \frac{dy}{y} = (2\pi)^{-s}L(s)G(s),$$

where

$$L(s) = \sum_{n=1}^\infty \frac{a_n}{n^s}$$

is the associated  $L$ -function, and

$$(2.4) \quad G(s) = \int_0^\infty K_{iR}(y)y^s \frac{dy}{y} = 2^{s-2}\Gamma\left(\frac{s+iR}{2}\right)\Gamma\left(\frac{s-iR}{2}\right).$$

Note that the series and integrals converge if  $\Re(s)$  is sufficiently large.

If  $f$  is odd then

$$(2.5) \quad (2\pi)^{-s}L(s)G(s+1) = \int_0^\infty \frac{\partial f}{\partial x}(iy)y^{s-\frac{1}{2}} \frac{dy}{y},$$

with  $L(s)$  and  $G(s)$  as before.

The key properties of  $L(s)$  are summarized in the following

**Proposition 2.1.**  $L(s)$  continues to an entire function which satisfies the functional equation

$$(2.6) \quad \begin{aligned} \xi(s) &= N^{-\frac{1}{4}+\frac{s}{2}}(2\pi)^{-s}L(s)G(s+a) \\ &= \pm(-1)^{a+1}\xi(1-s), \end{aligned}$$

where  $a = 0$  if  $f$  is even and  $a = 1$  if  $f$  is odd, the  $\pm$  is determined by the eigenvalue of  $f$  under the Fricke involution and whether  $f$  is even or odd, and  $G(s)$  is given in (2.4).

*Proof.* Let  $h$  equal  $f$  or  $\partial f/\partial x$ , depending on whether  $f$  is even or odd, respectively. Combining (2.3) or (2.5) with (2.2) we have

$$(2.7) \quad (2\pi)^{-s}L(s)G(s+a) = \int_\Delta^\infty h(iy)y^{s-\frac{3}{2}+a} dy \mp (-1)^a N^{\frac{1}{2}-s} \int_{\frac{1}{N\Delta}}^\infty h(iy)y^{-s-\frac{1}{2}+a} dy$$

for any  $\Delta > 0$ . By (8.2) the above integrals converge for any value of  $s$ , which proves the analytic continuation. Set  $\Delta = 1/\sqrt{N}$  to see that the right side satisfies the functional equation.  $\square$

### 3. LOCATING MAASS FORMS

thealgorithm)

Our goal is to find the first several Maass forms on various  $\Gamma_0(p)$ . In particular, we want to be sure that we are not missing any eigenvalues. The methods we use to locate Maass forms are similar to previous methods which have been used, such as that of Hejhal [Hej]. Indeed, our approach is quite similar to Hejhal's original collocation method, with the exception that we consider an overdetermined system of linear equations, and search for eigenvalues by detecting when the overdetermined system is close to consistent. We have found this approach to be more reliable than methods which detect eigenvalues by looking at properties of the coefficients. Although our system becomes ill-conditioned when we search for larger eigenvalues, and our coefficients lose precision slightly past the eigenvalue, these shortcomings are not in issue in the ranges we consider here. It would be possible to adapt Hejhal's [Hej2] later innovations to avoid these difficulties. In principle the method we describe works for

arbitrary cofinite subgroups of  $SL(2, \mathbb{R})$ , see [FL], although handling groups having more than one cusp is more difficult. Fredrik Strömberg [St] has developed algorithms which implement Hejhal's innovations and handle multiple cusps as well as characters.

Although we are concerned here with  $\Gamma_0(p)$ , we will describe the algorithm for an arbitrary cofinite group  $\Gamma$  with one cusp (recall that we have adjoined the Fricke involution to  $\Gamma_0(p)$ , the resulting group having one cusp). We will only outline the method, leaving details for another paper.

Given generators  $\{g_j\}$  of  $\Gamma$ , we wish to find functions  $f(z)$  of the form (2.1) so that  $f(g_j z) = f(z)$ . We use a truncation of the Fourier expansion of  $f$ :

$$(3.1) \quad \tilde{f}(z) = \sqrt{y} \sum_{|n| \leq M, n \neq 0} a_n K_{iR}(2\pi|n|y) \exp(2\pi i n x),$$

where the  $a_i$  are complex unknowns. Note that we assume  $a_0 = 0$  (which excludes all Eisenstein series when we have only one cusp) and also normalize one of the coefficients (usually  $a_1$ ) to equal 1. In addition, we rescale the  $K$ -Bessel function by multiplying by  $\exp(\pi R/2)$ , so  $K_{iR}(y)$  is oscillatory of size 1 for  $0 < y < R$ , and for larger  $y$  it decays exponentially, see (8.2). With these normalizations, and assuming a bound on the  $a_n$ , given  $R$  we can choose  $M$  so that  $|f(z) - \tilde{f}(z)|$  is as small as desired. For most of the examples in this paper, we choose  $M$  so that the error caused by the truncation is around  $10^{-8}$  for  $\Im(z) \geq Y_{MIN}$ . Here  $Y_{MIN}$  is chosen so that  $\Im(z) \geq Y_{MIN}$  for all  $z$  in a fundamental domain of  $\Gamma$ .

We treat the  $\{a_n\}$  as  $4M - 2$  real unknowns, and the new goal is to choose  $R$  such that there exists  $\{a_n\}$  so that  $\tilde{f}(g_j z) \approx \tilde{f}(z)$  for all the generators  $g_j$ . We do this by forming an overdetermined system of equations, depending on  $R$ , which will be close to consistent when  $R$  is an eigenvalue. Choose  $N$  points  $z_i$  (where  $N > 4M$ ) on a horizontal line  $Y_{MIN}$  in  $\mathbb{H}$ , where  $Y_{MIN}$  is lower down in the upper half plane than any point in a fundamental domain for  $\Gamma$ . (This is possible because we assumed  $\Gamma$  has one cusp). These points are mapped by the generators to points  $z_i^*$  in a fundamental domain for  $\Gamma$ . If  $f$  is a Maass form on  $\mathbb{H}/\Gamma$  then  $f(z_i) = f(z_i^*)$ , and  $\tilde{f}(z_i) \approx \tilde{f}(z_i^*)$ , where  $\approx$  stands for equality to within our truncation error. But we are thinking of  $R$  as fixed and the  $a_n$  as unknowns, so  $\tilde{f}(z_i) = \tilde{f}(z_i^*)$  is a linear equation in the  $a_n$ , which has the coefficients of a Maass form as a solution. The  $N$  equations

$$\tilde{f}(z_i) = \tilde{f}(z_i^*)$$

constitute an overdetermined system  $Ax = b$  in the  $4M - 2$  unknowns. So we are looking for "eigenvalues"  $R$  for which this system is consistent to within the error caused by the truncation. Note: this will find *all* eigenvalues. If one wishes to search only for newforms, then it is necessary to include additional equations to specify this. See [R].

Given a possible eigenvalue  $R$ , we determine the least square solution  $\tilde{x}$  (using  $QR$ -factorization) to this system of equations. We then use the norm of the error,  $\|A\tilde{x} - b\|_2$ , as a measure of how close  $R$  is to a true eigenvalue. If  $R$  is really an eigenvalue, then  $\|A\tilde{x} - b\|_2$  should be roughly the size of the truncation error. In our initial calculations of cases where earlier data were available we found this to be true. We also found that away from eigenvalues (i.e. if we choose  $R$  randomly) the error is generally of size 1, independent of the size of the truncation error. This is what one should expect for random  $R$ , given our rescaling of the  $K$ -Bessel function by the factor  $\exp(\pi R/2)$ .

We take  $\|A\tilde{x} - b\|_2$  to be a measure of distance between  $R$  and a “true” eigenvalue for  $\Gamma$ , and we have found this measure to vary smoothly and to be consistent with various other checks, which we describe below. Thus, it seems reasonable to say that when we find a value of  $R$  which gives a system that is consistent within our truncation error, we have found a function that is a factor of  $10^8$  closer to being invariant under  $\Gamma$  than a randomly chosen function.

When  $\|A\tilde{x} - b\|_2$  is less than our truncation error, we take the entries in  $\tilde{x}$  as the coefficients of our Maass form. Since  $K_{iR}(y)$  decays for  $y > R$ , we truncate our series at  $M$  somewhat larger than  $2\pi/Y_{MIN}$ . If  $\Gamma = \Gamma_0(p)$ ,  $p$  prime, then we can take  $Y_{MIN}$  to be anything smaller than  $\sqrt{3}/(2p)$ , and we usually take  $Y_{MIN} = 0.7/p$ . Note that for the coefficients near  $M$  we retain almost no precision. Indeed, because of the decay of the Bessel function the last several coefficients in  $\tilde{f}$  are inconsequential in the region  $\Im x > Y_{MIN}$ .

There are a number of error checks. Although we described the algorithm for arbitrary  $\Gamma$ , if  $\Gamma$  is arithmetic (as will be the case for the examples in this paper) then the Fourier coefficients will be multiplicative, and we find that the above method produces functions whose coefficients are multiplicative to better than the truncation error. These can be viewed as independent 1 in  $10^8$  error checks, which render it very likely that the functions produced are indeed Maass forms. In other words, the possibility of a “false alarm” is extremely small, and we have high confidence that, at least in the arithmetic case, the program is finding the Maass forms for  $\Gamma$ . Although we do not use the Hecke relations in our search, other approaches have used them to greatly speed up the calculations [BSS].

For nonarithmetic groups there are no Hecke relations, but there are other persuasive checks. We start with a general Fourier expansion with complex coefficients. For the Maass forms we find, the functions are real to very high accuracy (to an even higher accuracy than the truncation error). In general, when we are far from an eigenvalue, the system of equations is far from consistent and the approximate solutions are far from real.

A final check is the size of the Fourier coefficients. For arithmetic  $\Gamma$  all the coefficients we have found fit the Ramanujan-Peterson conjecture  $|a_p| < 2$ . For nonarithmetic groups that bound is not true in general, but it is still conjectured that  $a_n \ll n^\epsilon$ . And we do in fact find that if  $R$  is close to an eigenvalue then the  $a_n$  from the least-squares solution are much smaller (and not growing as a function of  $n$ ) than those from random  $R$ . We have been successful at using the *size* of the least-squares solution  $\tilde{x}$  as a measure of consistency of our overdetermined system  $Ax = b$ , although that approach does not seem as natural as directly measuring how close the system is to being consistent.

Our programs were implemented in Mathematica. Numerical calculations were all done to machine precision, which is 16 decimal digits on the computers we used. The most time consuming part of the calculation is the evaluation of the  $K$ -Bessel function. So for each value of  $R$  we wish to test, we speed up the calculation by first evaluating  $BesselK[IR, y]$  at a large number of  $y < R + 20$ , and then interpolating. For  $y > R + 20$ , where the Bessel function is decaying exponentially, we use an asymptotic formula.

#### 4. LOW EIGENVALUES FOR $\Gamma_0(p)$

(eigenvalues) In Table 1 we present the first eigenvalue in each of the four symmetry types for  $\Gamma_0(p)$ ,  $p$  prime.

Table 1 shows a few trends. For example, the first (*even, +*) eigenvalue tends to be smaller than the first (*even, -*) eigenvalue. This is not surprising because the number of

| $p$ | (even, +)       | (even, -)       | (odd, -)        | (odd, +)        |
|-----|-----------------|-----------------|-----------------|-----------------|
| 2   | 8.9228764869917 | 12.092994875078 | 7.220871975958  | 5.4173348068447 |
| 3   | 5.0987419087295 | 8.7782823935545 | 6.1205755330872 | 4.3880535632221 |
| 5   | 4.1324042150632 | 5.436180461416  | 4.897235015733  | 3.028376293066  |
| 7   | 3.454226503571  | 4.8280076684720 | 4.119009292925  | 1.924644305111  |
| 11  | 2.4835910595550 | 4.018069188221  | 2.96820576382   | 2.033090993855  |
| 13  | 2.025284395696  | 3.701627575242  | 2.8308066514473 | 0.97081541696   |
| 17  | 1.849687906031  | 3.169382380088  | 1.967986359638  | 1.441428545022  |
| 19  | 1.32979889046   | 3.0371960205    | 2.297006359074  | 1.09199155992   |
| 23  | 1.57958924015   | 2.61095996203   | 1.393337141483  | 1.5061266371    |
| 29  | 1.01726655080   | 2.35848525400   | 1.4875542669    | 1.21206072002   |
| 31  | 0.78935617774   | 2.3681029381    | 1.68678370214   | 1.06284037124   |
| 37  | 1.22324304054   | 2.07459336618   | 1.7095550812    | 0.6423059582    |
| 41  | 0.66572483212   | 2.00647646730   | 1.20439574249   | 0.86739746584   |
| 43  | 1.10814196343   | 1.80282682958   | 1.33429136841   | 0.65545238186   |
| 47  | 1.11157408467   | 1.6028012074    | 0.5854521430    | 1.2635566239    |
| 53  | 1.0158404282    | 1.49379571497   | 1.10150481917   | 0.8039894596    |
| 59  | 0.59582968816   | 1.7096938151    | 0.5985969867    | 1.0391204647    |
| 61  | 0.67704450723   | 1.7475722491    | 1.40716257846   | 0.41806231115   |
| 67  | 0.84247476      | 1.3611564746    | 1.0195601623    | 0.6775902092    |
| 71  | 0.3574504906    | 1.579666665     | 0.5829071706    | 1.02176122015   |
| 73  | 0.654548913     | 1.402091810     | 1.3304765833    | 0.5178875052    |
| 79  | 0.5517748428    | 1.5496128514    | 0.9963893608    | 0.7490008694    |
| 83  | 0.817132725     | 1.0975181181    | 0.6402875784    | 0.9518887750    |
| 89  | 0.489435980     | 1.4372631258    | 0.860333981     | 0.688804233     |
| 91  | 0.6038860327    | 1.206246429     | 1.132502360     | 0.416931671     |
| 101 | 0.453759608     | 1.30563134      | 0.546229605     | 0.77990698      |
| 103 | 0.685190643     | 1.08157342      | 0.724051309     | 0.56540244      |
| 107 | 0.840011226     | 0.90440769      | 0.581677094     | 0.90574018      |

(tab:lowest) TABLE 1. First eigenvalue,  $R$ , in each of the four symmetry types of  $\Gamma_0(p)$ , for prime  $p \leq 107$ . Values shown are truncations of the actual values, and all digits are believed to be correct.

nodal domains is an increasing function of the eigenvalue, and the symmetry relations force various constraints on the nodal curves. This also has an effect on the lower order terms in Weyl's law, which can be seen in Table 2.

To further study the low eigenvalues, we considered the normalized eigenvalues  $\tilde{\lambda} = \frac{p+1}{12}R^2$ , where  $\frac{p+1}{12}$  is the (reciprocal of the) coefficient of the leading term in Weyl's law, so that  $\tilde{\lambda}_n \sim n$  for the  $n$ th eigenvalue. Figure 1 shows the cumulative distribution functions of the first  $\tilde{\lambda}$  in each symmetry type: the horizontal axis are the normalized first eigenvalue  $\tilde{\lambda} = \frac{p+1}{12}R^2$ , and the vertical axis is the fraction of  $p$  in our data set having a smaller normalized first eigenvalue. If each symmetry type was equally likely to have the lowest eigenvalue then each plot would correspond to a density with mean 4. This is not the case, for the reasons described in the previous paragraph. A more sophisticated normalization, involving the lower order terms in Weyl's law, would be needed in order to reveal any underlying structure.

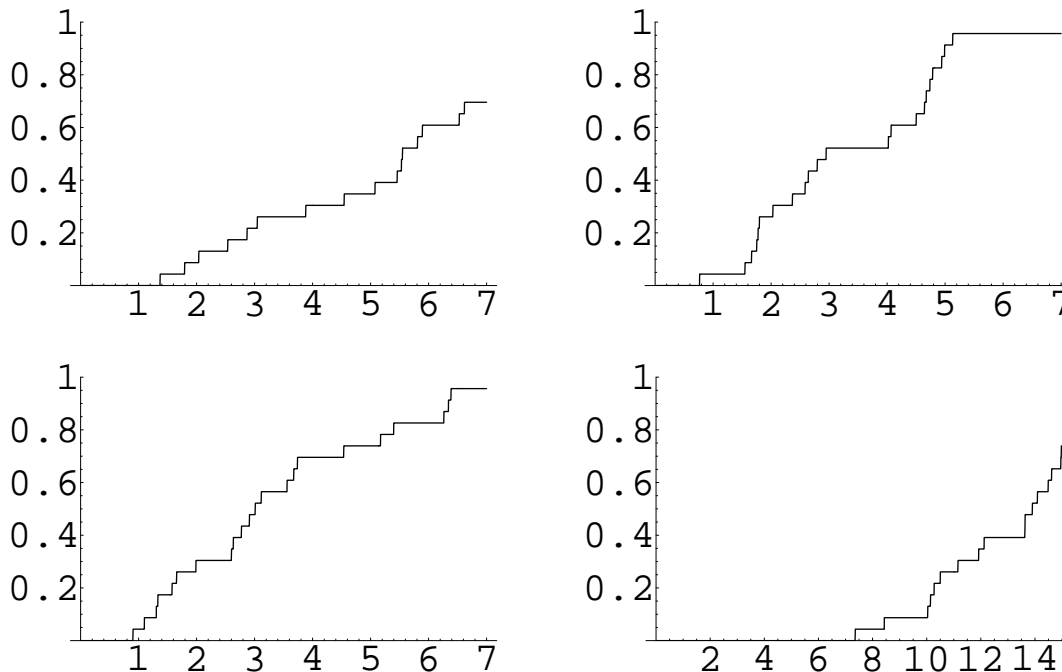


FIGURE 1. Cumulative distributions of the rescaled first eigenvalue in each of the four symmetry types for  $\Gamma_0(p)$ . Clockwise from top left we have odd plus, even plus, even minus, and odd minus.

### 5. THE FIRST 1000 MAASS FORMS ON $\Gamma_0(11)$

We applied the method described in the previous sections to find all Maass newforms on  $\Gamma_0(11)$  with  $R < 36.5$ , resulting in a total of 1054 eigenvalues. The first 30 eigenvalues in each symmetry type are given in Table 2. We have verified that the methods described in the previous section work for  $R \approx 100$  for  $\Gamma_0(11)$ . Possibly they work for  $R \approx 500$  but probably not for  $R \approx 1000$ . The limitations here are caused by the ill-conditioning of the linear system. Hejhal’s improvements [Hej2] have been implemented by Fredrik Strömberg [St], which eliminates this ill-conditioning. For those methods, computer time and memory become the constraint. From the calculations of Then [Th], one might expect that for  $\Gamma_0(11)$  those refinements could explore  $R$  a bit larger than 10,000.

**5.1. Weyl’s law justification that the list is complete.** It is natural to question whether our list of 1000 eigenvalues is complete. It is possible to do a calculation using the trace formula to justify this assertion, as in [BS, BSV]. However, we will use a simpler but less rigorous method involving Weyl’s law. This approach is well known to physicists and we do not claim that any of the ideas in this section are new. In particular, this method was used in [BSS] to check that a list of large eigenvalues of the full modular group did not have any gaps.

The method we describe is quite robust and does not require any *a priori* knowledge about the eigenvalue counting function. In addition to checking lists of eigenvalues, the method also works well for zeros of  $L$ -functions, zeros of derivatives of  $L$ -functions, and no doubt many

| $(\text{even}, +)$ | $(\text{even}, -)$ | $(\text{odd}, -)$ | $(\text{odd}, +)$ |
|--------------------|--------------------|-------------------|-------------------|
| 2.48359105931      | 4.01806918817      | 2.03309099399     | 2.96820576406     |
| 3.28347243577      | 4.55526078519      | 3.03251283477     | 3.67969872541     |
| 4.71167698688      | 5.763876683        | 3.48188847623     | 4.52889442543     |
| 4.93319801514      | 6.24170090061      | 4.47950391861     | 5.38428160742     |
| 5.26506649404      | 6.50705758603      | 4.73801386035     | 5.86853222013     |
| 5.98954160832      | 7.16536040411      | 4.96681056818     | 6.03361084498     |
| 6.53884437369      | 7.73368897382      | 5.66326548842     | 6.77549239897     |
| 6.61367515372      | 7.88007383371      | 6.06921835945     | 7.02463370057     |
| 7.26644184877      | 8.62006794999      | 6.58162198432     | 7.59926619568     |
| 7.57048468847      | 8.99092809554      | 6.83944314323     | 7.68091057664     |
| 8.1420217952       | 9.10172820901      | 7.29898901659     | 8.43825975028     |
| 8.2745067789       | 9.22640277057      | 7.48914848604     | 8.55580430772     |
| 8.51378467778      | 9.58661569223      | 7.51799881213     | 8.57197306999     |
| 8.67868612906      | 10.1232769351      | 8.04940484112     | 9.04133195689     |
| 9.34515203418      | 10.3790777119      | 8.16066289206     | 9.46659932758     |
| 9.58209996953      | 10.6466817416      | 8.65213300992     | 9.58865618615     |
| 9.67447022214      | 10.9372887384      | 8.92993868939     | 10.1617823366     |
| 9.86213636813      | 11.1472353004      | 9.19975228208     | 10.2760011943     |
| 9.98570867995      | 11.4784159679      | 9.67408869747     | 10.6445164137     |
| 10.6430998724      | 11.785015526       | 9.70588526636     | 10.6694194813     |
| 10.6895930795      | 11.8109636758      | 9.85493309024     | 10.989904792      |
| 11.1502516477      | 12.0601741852      | 10.1854915198     | 11.2612425027     |
| 11.1780820772      | 12.6105517277      | 10.3386794422     | 11.2733375812     |
| 11.4741161917      | 12.6118028204      | 10.5313292208     | 11.8005163423     |
| 11.6836999337      | 12.9273387317      | 10.8165867701     | 11.8348731714     |
| 11.9293065449      | 12.9741004148      | 10.9051400611     | 11.9611740135     |
| 12.038113214       | 13.1014471689      | 11.3280653248     | 12.2747697039     |
| 12.3049680989      | 13.3464693158      | 11.5395912507     | 12.6217030476     |
| 12.5345178216      | 13.9313207377      | 11.6712226728     | 12.8306123388     |
| 12.6348846255      | 13.9973467855      | 11.7801194448     | 13.0161442996     |

TABLE 2. First 30 newform eigenvalues in each symmetry type of  $\Gamma_0(11)$ .  
 Values shown are truncations of the actual values, and all digits are believed to be correct. Note that there are only three oldforms in the range covered by the table: an even oldform at  $R \approx 13.779751$ , and odd oldforms at  $R \approx 9.533695$  and  $R \approx 12.173008$ .

other cases. In some of those cases we know very precise information about the counting function of the objects being studied, but this is not necessary for the method.

Let  $N(x) = \#\{\lambda_j : 0 < \lambda_j \leq x\}$ . The method is based on the assumption that there exists a nice function  $f$ , which is of a fairly simple form, such that

$$(5.1) \quad r(x) := N(x) - f(x)$$

grows very slowly and averages to 0 over small intervals. Weyl's law provides the leading order behavior of  $f(x)$ , and it is conjectured that there are lower order terms of the form  $\sqrt{x} \log(x)$ ,  $\sqrt{x}$ , and perhaps  $x^{\frac{1}{4}}$  or  $\log(x)$ . But it is not known that such lower order terms exist: proving such terms would greatly improve the known bounds on the multiplicity of eigenvalues of the Laplacian. For our calculation we *assume* that such a refined Weyl's law

exists. It is also necessary for this method that the first few eigenvalues have been found: the method only detects missing eigenvalues in the “middle” of the spectrum.

We justify that our list of eigenvalues is complete in two steps:

- demonstrate that the function  $f$  exists for our claimed complete list of eigenvalues.
- demonstrate that the function  $f$  does not exist for lists with missing eigenvalues.

First we consider the case of all newforms on  $\Gamma_0(11)$ , and we assume that the function  $f$  has the form  $f(x) = Ax + B\sqrt{x}$ . If we choose  $A$  and  $B$  to give the best least-squares fit we find  $A = 0.83305$  and  $B = -1.51762$ . This shows good agreement with the known main term of  $A = 10/12 \approx 0.83333$ . Figure 2 plots the function  $r(x)$  from equation (5.1), as well as  $r(x)$  averaged over a moving window of width 150. The horizontal axis is the eigenvalue for  $0 < \lambda < 1200$ , and the vertical axis is  $r(\lambda)$ . The “fingerprint” structure in the first graph is just an artifact of how the plots were generated.

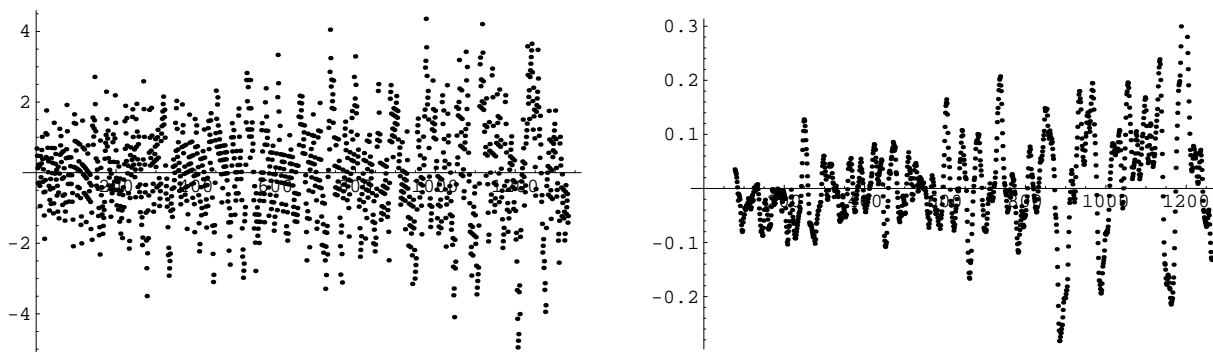


FIGURE 2. The remainder function  $r(x)$  defined in (5.1) where  $f(x)$  is chosen as described in the text. The data is the 1054 newforms on  $\Gamma_0(11)$  with  $\lambda < 1260$ . The plot on the right is the running average over a window of length 150.

(fig:weylall)

As can be seen, the function  $r(x)$  is small, and it is also small on average.

We now repeat the calculation on a list of eigenvalues which is known to be incomplete, to demonstrate how the method detects the missing value. In Figure 3 we consider the eigenvalues in the  $(\text{even}, -)$  space, for which we have removed one eigenvalue  $\lambda \approx 510$ . Since we are in the  $(\text{even}, -)$  space, there are only  $1/4$  as many eigenvalues, so it should actually be easier to fit a main term function  $f(x)$ . We want to make the point that is impossible to find functions  $f$  and  $r$  for this list of data, because the missing eigenvalue causes a “step” in the counting function that cannot be absorbed by a nice function. We choose  $f$  of the form

$$(5.2) \quad f(x) = Ax + B\sqrt{x} \log x + C\sqrt{x} + Dx^{\frac{1}{4}} + E \log x + F,$$

and then choose  $A, B, C, D, E, F$  to give the best least-squares fit. The resulting  $r(x)$  and  $r(x)$  averaged over a window of size 150 is shown in Figure 3.

As can be seen, in Figure 3  $r(x)$  does not average to zero over small intervals, and in fact we can almost read off the missing value  $\lambda \approx 510$  from the averaged graph. It is also interesting that without averaging it is difficult to see the missing eigenvalue in the plot of  $r(x)$ . The fact that we fit a function with many free parameters is meant to suggest the robustness of the method. Unfortunately, when fitting such a general function to such a small amount of data, we can no longer use the coefficient  $A$  of the main term to check the known main term in Weyl’s law.

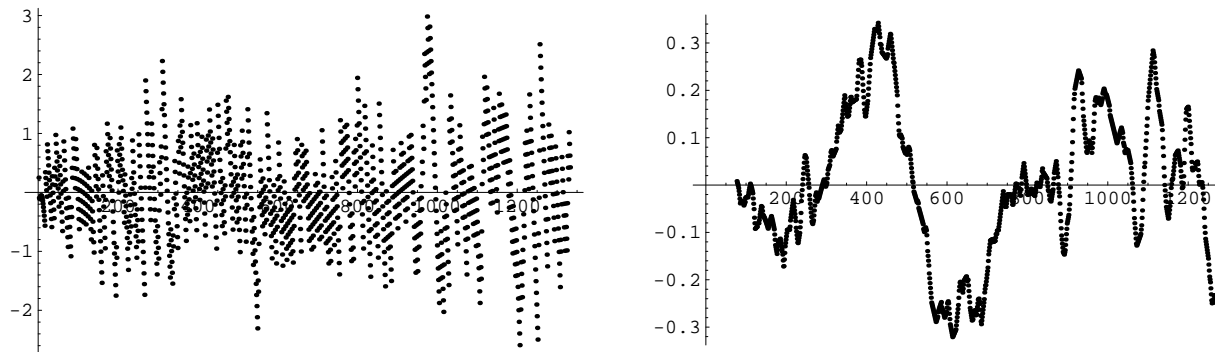


FIGURE 3. The remainder function  $r(x)$  for the first 250 (even,  $-$ ) newform eigenvalues on  $\Gamma_0(11)$ , where *one eigenvalue with  $R^2 \approx 510$  has been intentionally omitted*. The plot on the right is the running average over a window of length 150.

(fig:weylem)

**5.2. Shortcomings of the method.** There are some obvious shortcomings of the method of fitting Weyl’s law to check the data.

First, the method cannot detect missing eigenvalues at the beginning of the list. Such missing terms are absorbed by the constant term in our function.

Second, if a large number of eigenvalues are missing, and the missing eigenvalues are very regularly spaced, then this may not be detected. Indeed, that is exactly the situation at hand. We are claiming to justify that our list of *newform* eigenvalues is complete. But if we were mistakenly claiming that we had the list of *all* eigenvalues, that error would not be immediately caught by our fit to “Weyl’s law,” for the missing eigenvalues, i.e. the oldforms, have their own Weyl’s law. In the case here, we know the coefficient of the main term in the counting function for newforms, and our fit function shows good agreement with that. However, we cannot rule out the possibility that we are systematically missing every 100th eigenvalue, for example.

**5.3. Statistics of the eigenvalues.** It is generally believed that the newform eigenvalues in each symmetry class are as uncorrelated as possible (have Poisson statistics), the newform eigenvalues in the different symmetry classes are uncorrelated, and there is no correlation between newform eigenvalues and oldform eigenvalues. For the case of  $SL(2, \mathbb{Z})$  these conjectures are strongly supported by numerical evidence [BSS]. (We presume that Dennis Hejhal has also made such statistical tests, but we were unable to locate a reference). We now check if our data supports these conjectures. Only the case of the spacing of oldforms within the list of newforms can be considered new here.

In Figure 4 we consider the nearest neighbor spacing of the eigenvalues on  $\Gamma_0(11)$ , both for the full spectrum and for one particular symmetry type. Good agreement with Poisson statistics is found.

Next we consider the location of the oldforms in among the newforms. If there is no correlation then the oldforms should be distributed uniformly between the two neighboring newforms. Figure 5 shows the (scaled) location of the oldforms between the neighboring newforms, giving a good agreement with the expected Poisson distribution. That is, for each oldform eigenvalue  $R_{old}$  we locate the neighboring newform eigenvalues  $R_j < R_{old} < R_{j+1}$ . We then consider the relative location of the old eigenvalue  $R_{old}^* = (R_{old} - R_j)/(R_{j+1} - R_j)$ ,

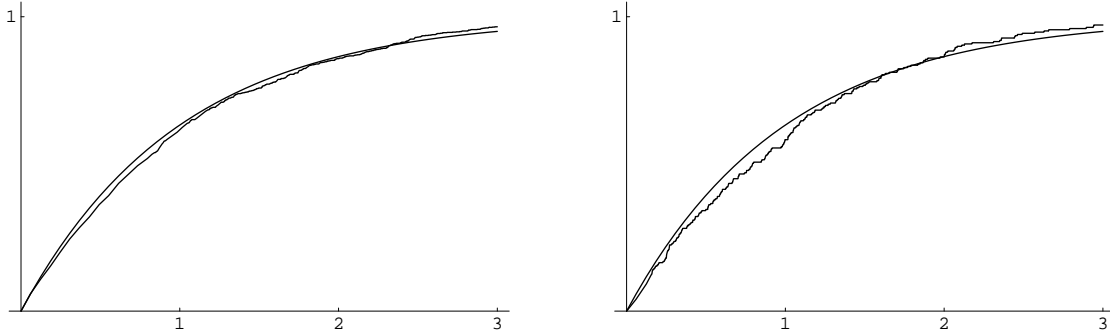


FIGURE 4. Cumulative distribution of normalized nearest neighbor spacing of newforms on  $\Gamma_0(11)$ . The smooth curve is the cumulative distribution for Poisson spacing. The plot on the left is for all newforms and the plot on the right is for (even,  $-$ ) forms.

(fig:eignn)

which lies in the interval  $(0, 1)$ . Each  $R_{old}^*$  in the range of our data is shown in Figure 5, and the straight lines correspond to a Poisson (uniform) distribution.

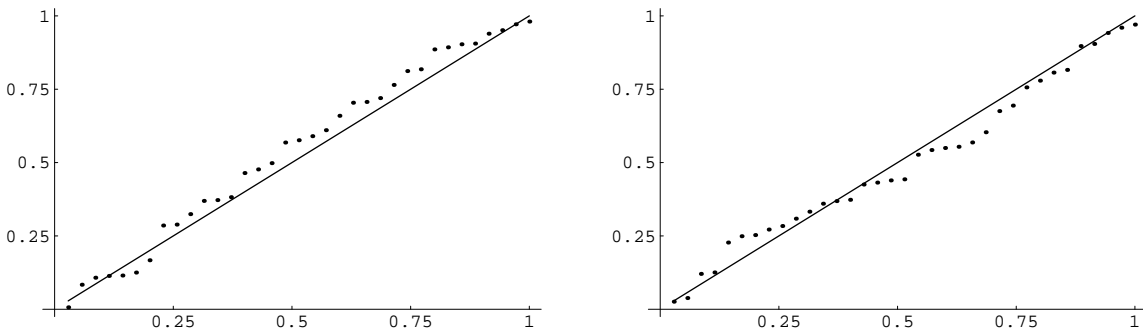


FIGURE 5. Ordered normalized location of odd oldforms within neighboring newforms, for the 35 oldforms with  $R < 36.5$ . Straight line is comparison to random (Poisson) spacing. The plot on the left is for odd $-$ , on the right for odd $+$ .

(fig:oldodd)

## 6. EXAMPLE MAASS $L$ -FUNCTIONS

(sec:examples)

We give example plots of Maass  $L$ -functions and discuss some general features, and in the next section we consider the statistics of zeros and critical values. Maass form  $L$ -functions were first evaluated by Strömbergsson [S] for some Maass forms on the full modular group.

By the functional equation,  $\xi(\frac{1}{2} + it)$  is real for real  $t$ , so there is a simple rescaling (involving a ratio of  $\Gamma$ -functions) to produce a function with the same modulus as  $L(\frac{1}{2} + it)$  which is real for real  $t$ . It is that real function of the real variable  $t$ , which we still call “the  $L$ -function”, which is shown in Figure 6. There are four classes of  $L$ -functions, depending on whether the function  $f$  is even or odd as a function of  $x$ , and whether  $f$  has eigenvalue  $+1$  or  $-1$  under the Fricke involution. One example of each combination is shown in Figure 6.

The first thing to notice is that these plots make it appear that the Riemann hypothesis is false for these  $L$ -functions. For example, in the upper-right plot, the negative local maximum near  $t = 5$  indicates a zero off the critical line. However, that zero off the line is a trivial zero, which has imaginary part  $iR$ , so this is not a counterexample to the Riemann Hypothesis.

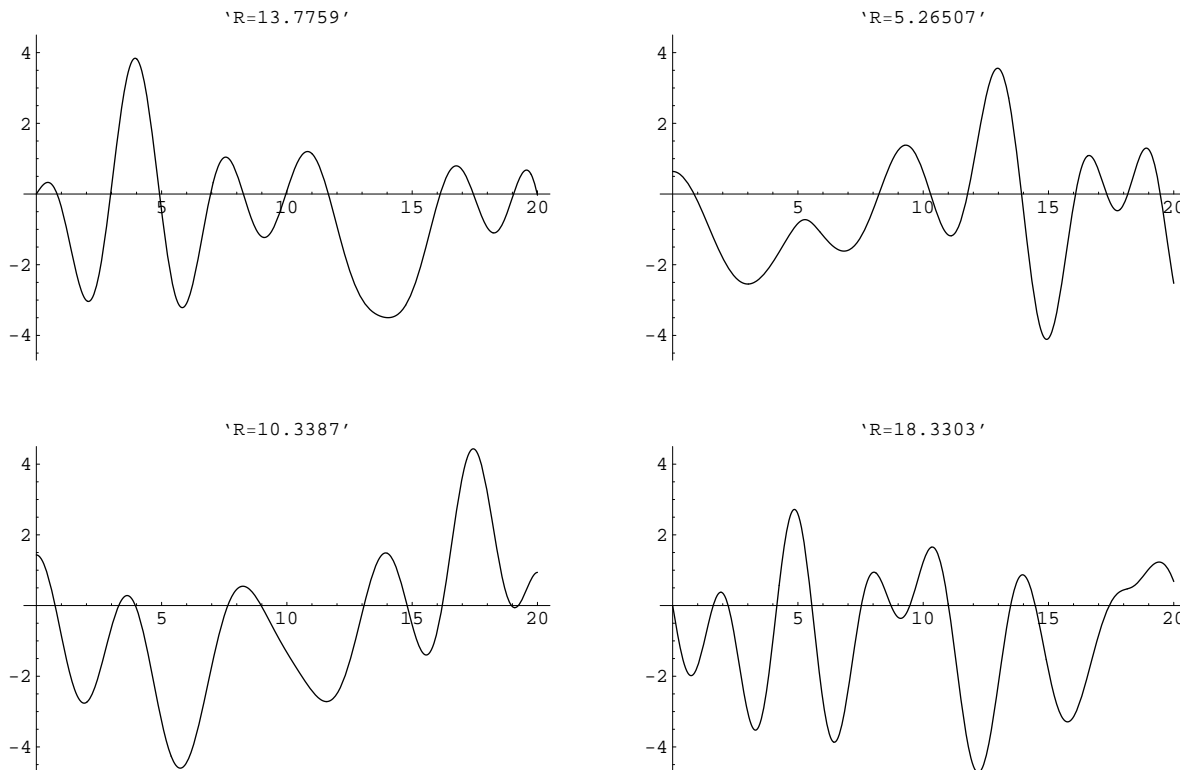


FIGURE 6. Plots of (the real version of)  $L(\frac{1}{2} + it)$ , one for each of the four symmetry types of Maass forms on  $\Gamma_0(11)$ . Clockwise from top left we have odd minus, odd plus, even plus, and even minus. Each plot is labeled with the “eigenvalue”  $R$  of the Maass form.

(fig:fourplots)

The effect of the trivial zeros is more noticeable in the even case, where they are closer to the critical line. This illustrates Strömbergsson’s [S] observation of a gap in critical zeros near  $t = R$ .

The average spacing of zeros is a function of both  $R$  and  $t$ , the precise dependence can be deduced from the functional equation and the argument principle. For our purposes it suffices to note that for  $|t| < R$  the zero spacing is primarily a function of  $R$ , increasing with  $R$ , except for a slight decrease in density near  $|t| = R$ .

The number  $\varepsilon := \pm(-1)^{a+1}$  from (2.6) is called “the sign of the functional equation.” If  $\varepsilon = +1$  then  $L(\frac{1}{2}) \geq 0$ , and we call  $L(\frac{1}{2})$  the “critical value”. If  $\varepsilon = -1$  then  $L(\frac{1}{2}) = 0$  and  $L'(\frac{1}{2})$  is the critical value.

## 7. CHECKING THE RANDOM MATRIX PREDICTIONS

(sec:data)

Random Matrix Theory has become a fundamental tool for understanding the zeros of  $L$ -functions. Montgomery [Mon] showed that (in a limited range) the two-point correlations between the non-trivial zeros of the Riemann  $\zeta$ -function is the same as that of the eigenvalues of large random unitary matrices, and he conjectured that the correlations were in fact equal. There is extensive numerical evidence [Odl] in support of this conjecture, and in particular many statistics of the zeros of the  $\zeta$ -function, such as the distribution of nearest neighbor spacing, are believed to be the same as that of large random unitary matrices.

Katz and Sarnak [KSa] introduced the idea of studying zero distributions within families of  $L$ -functions and have conjectured that these coincide with the eigenvalue distributions of the classical compact groups: unitary, symplectic, and orthogonal. For these groups the averaged eigenvalue distributions are the same (in the limit of large matrix size), it is the eigenvalues near 1 which have different distributions in each case. In terms of  $L$ -functions this corresponds to zeros near the critical point, so our concern is with the low lying zeros.

The family of Maass  $L$ -functions is an Orthogonal family (see [CFKRS]), which we further break into  $O^+ = SO(\text{even})$  and  $O^- = SO(\text{odd})$ , depending on whether the  $L$ -function has sign  $+1$  or  $-1$  in its functional equation. In the latter case  $L(\frac{1}{2}) = 0$ , which corresponds to the fact that odd orthogonal matrices have 1 as an eigenvalue.

In Figure 7 we consider the distribution of the height of the first zero above the critical point, comparing to the analogous quantity for eigenvalues of orthogonal matrices. In Fig-

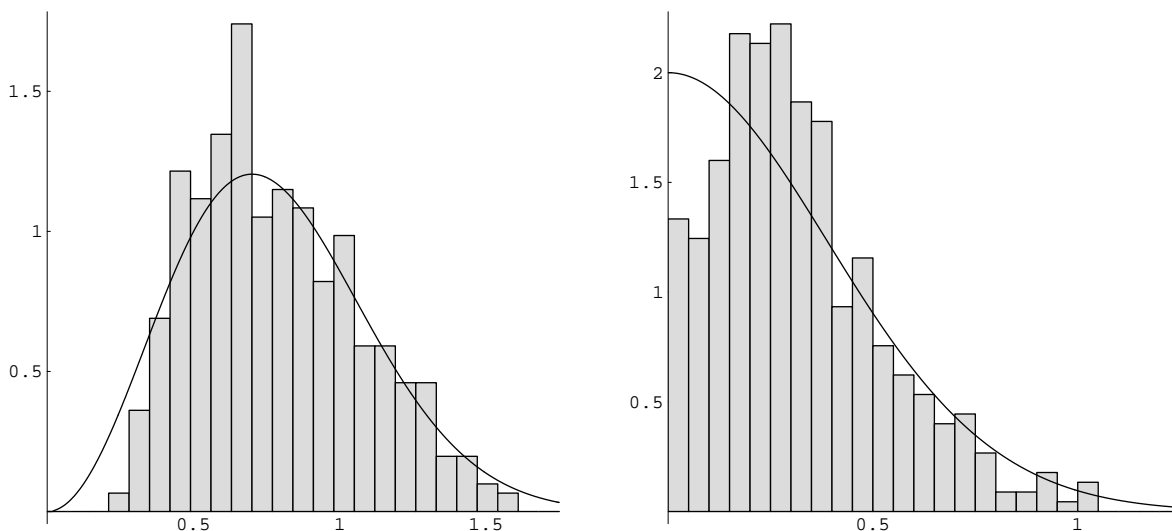


FIGURE 7. Density of first zero above the critical point for 435  $L$ -functions from  $\Gamma_0(11)$  with  $\varepsilon = -1$  on the left, and 450 with  $\varepsilon = +1$  on the right. The continuous curves are the densities for the corresponding eigenvalues for  $O^-$  and  $O^+$ , respectively. The  $L$ -function zeros have been rescaled to have the same averages as the corresponding eigenvalues.

g:firstzeros)

ure 7 we omit the Maass forms with  $R < 15$ , because the small values of  $R$  cause anomalous behavior of the first few zeros.

Next we show the cumulative distribution of the critical values, fit to the prediction from random matrix theory. In the case of even functional equation, corresponding to  $O^+$  matrices, the density of critical values scales as  $c/\sqrt{x}$  for small  $x$ . This is quite difficult to see in a histogram, so instead we consider the cumulative distribution and compare to the predicted  $c'\sqrt{x}$ , where we choose  $c'$  by fitting to the data. Figure 8 shows very good agreement.

In Figure 8 we omit the first 30 Maass forms of each symmetry type, corresponding to approximately  $R < 13$ , because the small values of  $R$  cause anomalous behavior near the critical point.

In the case of odd functional equation,  $\varepsilon = -1$ , the density of small values is predicted to scale as  $cx^{3/2}$ . In particular, there should be very few small values. Indeed we find very few

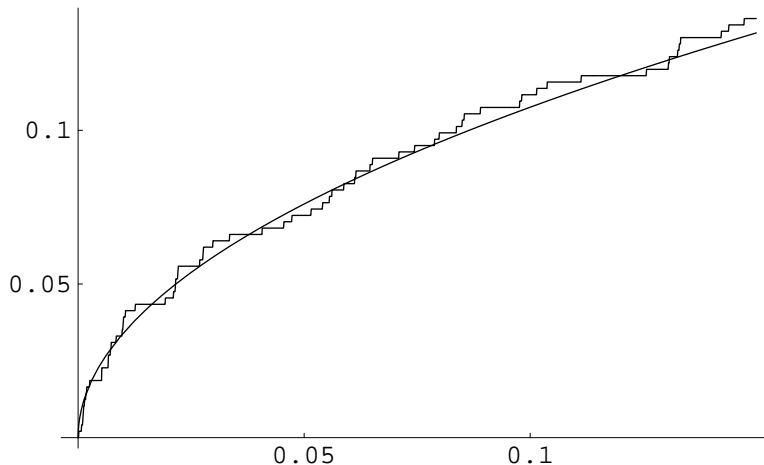
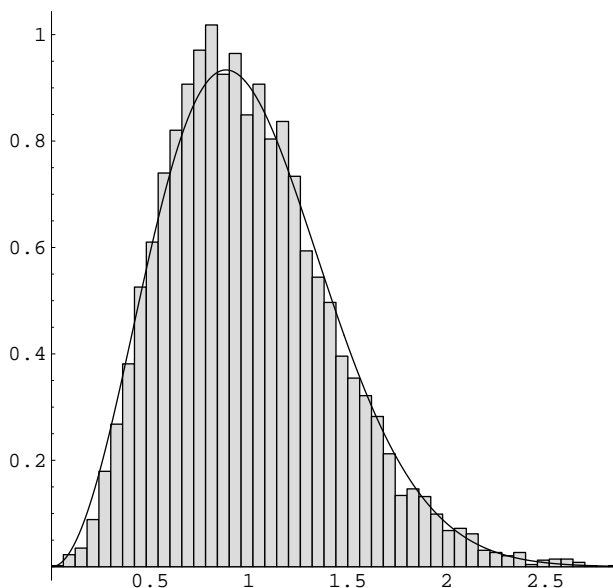


(fig:critical1) FIGURE 8. Cumulative distribution of critical values for  $\varepsilon = +1$   $L$ -functions. A total of 484  $L$ -functions were considered, of which 63 feature in this plot. The continuous curve is  $0.34\sqrt{x}$ .

cases where  $L'(\frac{1}{2})$  is small, but our statistics are too low to make a meaningful comparison with the random matrix prediction.

Finally, we show the distribution of nearest neighbor spacings. In Figure 9 we consider Maass forms with  $R > 21.5$ , and we considered the neighbor gaps between zeros starting with the 5th zero and going up to  $t = 20$ . This was designed to avoid the anomalous behavior near the critical point and near  $t = R$ . The fit to the random matrix prediction in Figure 9



restneighbor) FIGURE 9. Nearest neighbor gaps, normalized to remove the dependence on  $R$  and  $t$ . A total of 8086 neighbor gaps from approximately 650  $L$ -functions. The continuous curve is the normalized nearest neighbor spacing of eigenvalues of large random unitary matrices.

is quite good. Indeed this may be somewhat surprising because the zeros considered there lie in the range  $|t| < R$ , which one might expect to be different from the  $t \rightarrow \infty$  case. Perhaps this illustrates the universality of the random matrix behavior.

## 8. COMPUTING $L(s)$

`ec:computing`) Our interest is in the low-lying zeros of  $L(s)$ , so we only require an efficient method of evaluating  $L(\sigma + it)$  for small  $t$ .

Substituting (2.1) in to (2.7), and then switching the order of summation and integration, we have

$$\begin{aligned}
 (2\pi)^{-s} L(s) G(s+a) &= (2\pi)^{(2a-1)(s)} \sum_{n=1}^{\infty} a_n n^{(2a-1)(s)} \int_{2\pi n \Delta}^{\infty} K_{iR}(y) y^{s+(a-1)} dy \\
 &\quad \pm (-1)^{a+1} N^{\frac{1}{2}-s} (2\pi)^{(1-s)(2a-1)} \sum_{n=1}^{\infty} a_n n^{(1-s)(2a-1)} \int_{2\pi n/N\Delta}^{\infty} K_{iR}(y) y^{a-s} dy \\
 &= (2\pi)^{-s} \sum_{m=1}^{\infty} \left( \sum_{n=1}^m a_n n^{-s} \right) \int_{2\pi m \Delta}^{2\pi(m+1)\Delta} K_{iR}(y) y^{s-1+a} dy \\
 (8.1) \quad \{?\} &\quad \pm (-1)^{a+1} N^{\frac{1}{2}-s} (2\pi)^{s-1} \sum_{m=1}^{\infty} \left( \sum_{n=1}^m a_n n^{s-1} \right) \int_{2\pi m/N\Delta}^{2\pi(m+1)/N\Delta} K_{iR}(y) y^{a-s} dy
 \end{aligned}$$

We use the above expression, truncating the sum over  $m$ , in our calculations.

To decide where to truncate the sum, we use the estimate

$$(8.2) \quad \boxed{\text{eqn:kdecay}} \quad K_{iR}(y) \approx \sqrt{\frac{\pi}{2y}} e^{-y} e^{\frac{\pi R}{2}},$$

for  $y > 2R$ . We also must assume a bound on the coefficients  $a_n$ . It is conjectured that  $|a_n| \leq d(n)$ , where  $d(n)$  is the number of divisors of  $n$ . That bound is far from being proven, but since it holds for all coefficients which have been computed, we assume it in our estimates. Finally, to isolate  $L(s)$  we must divide the above expression by  $(2\pi)^{-s} G(s+a)$ . This increases the required precision because  $G(s)$  decays rapidly as  $\Im(s)$  increases. However, this will not be an issue because our concern is with low-lying zeros.

The Bessel function  $K_{iR}(y)$  oscillates rapidly as  $y \rightarrow 0$ , so it is desirable to have the lower limit of integration as high as possible. This is accomplished by choosing  $\Delta = 1/\sqrt{N}$ . Since  $\Delta$  is a free variable, we implemented an error check that looks for differences in  $L(s)$  when different values of  $\Delta$  are used, finding good agreement.

Note that this approach is useless for  $t > R$  because there is catastrophic cancellation in the sums. Note also that the number of coefficients we obtain for our Maass form is more than adequate for the range  $t < R$ . This is because the  $L$ -function requires  $f(iy)$  for  $y > 1/\sqrt{N}$ , and if the level  $N$  is prime we choose the number of terms so that we have an accurate evaluation of  $f(iy)$  for  $y > Y_{MIN} = 0.7/N$ . Additionally, if  $R$  were large it will be very time consuming to numerically integrate the  $K$ -Bessel function. More sophisticated methods [Rub] can overcome all of these difficulties.

We used the above considerations to produce  $L$ -functions values with an error of approximately  $10^{-6}$ , for  $t$  up to  $\min(20, R)$ . Since we only seek data to produce statistics involving neighbor spacing and value distributions, this level of accuracy is more than adequate. If one

wanted to study many zeros of a single  $L$ -function then more sophisticated methods would be needed.

## REFERENCES

- [CFKRS] [CFKRS] J.B. Conrey, D.W. Farmer, J. Keating, M. Rubinstein, and N.C. Snaith, “Integral moments of  $L$ -functions”, Proc. Lond. Math. Soc. 91 (2005) 33104. math.NT/0206018 .
- [BSS] [BSS] J. Bolte, G. Steil, and F. Steiner, *Arithmetical chaos and violation of universality in energy level statistics*, Phys. Rev. Lett. 69, 1992, 2188–2191.
- [BSV] [BSV] A. Booker, A. Strömbergsson, A. Venkatesh, *Effective Computation of Maass Cusp Forms*, preprint.
- [BS] [BS] A. Booker and A. Strömbergsson, *Numerical computations with the trace formula and the Selberg eigenvalue conjecture*, preprint.
- [FL] [FL] D. W. Farmer and S. Lemurell. *Deformations of Maass forms*, Math. Comp. 74 (2005) 1967-1982, math.NT/0302214
- [Hej] [Hej] D. Hejhal, *Eigenvalues of the Laplacian for Hecke triangle groups*. Mem. Amer. Math. Soc. 97 (1992), no. 469, vi+165 pp.
- [Hej2] [Hej2] D. Hejhal, *On eigenfunctions of the Laplacian for Hecke triangle groups*, In Emerging applications of number theory (Minneapolis, MN, 1996).
- [Iw] [Iw] Iwaniec, Henryk, Spectral methods of automorphic forms. Second edition. Graduate Studies in Mathematics, 53. American Mathematical Society, Providence, RI; Revista Matemática Iberoamericana, Madrid, 2002.
- [KSa] [KSa] N. M. Katz and P. Sarnak, Random matrices, Frobenius eigenvalues, and monodromy, AMS Colloquium Publications, 45 AMS, Providence, RI 1999.
- [Mon] [Mon] H.L. Montgomery, *The pair correlation of zeros of the Riemann zeta-function*, Proc. Symp. Pure Math. 24 1973 pp. 181-93.
- [Odl] [Odl] A. Odlyzko, *The  $10^{20}$ th zero of the Riemann zeta-function and 70 million of its neighbors.*, Preprint 1989.
- [R] [R] Rankin, Robert A. Modular forms and functions. Cambridge University Press, Cambridge-New York-Melbourne, 1977.
- [Rub] [Rub] M. Rubinstein, Computational methods and experiments in analytic number theory, preprint, math.NT/0412181
- [St] [St] F. Strömberg, Computational Aspects of Maass Waveforms, thesis, Uppsala Universitet, 2005.
- [S] [S] A. Strömbergsson, *On the Zeros of  $L$ -Functions Associated to Maass Waveforms* International Mathematics Research Notices, 15 1999, 839–851
- [Th] [Th] H. Then, *Maass cusp forms for large eigenvalues*, Math. Comp. 74 (2005), no. 249, 363381

AMERICAN INSTITUTE OF MATHEMATICS  
360 PORTAGE AVE.  
PALO ALTO, CA 94306  
FARMER@AIMATH.ORG

CHALMERS UNIVERSITY OF TECHNOLOGY,  
SE-412 96  
GÖTEBORG, SWEDEN  
SJ@MATH.CHALMERS.SE